Multi-path propagation in on-chip optical wireless links

(Article begins on next page)

Multi-Path Propagation
in On-chip Optical Wireless Links

Jacopo Nanni, Gaetano Bellanca, Giovanna Calò, Badrul Alam, Ali Emre Kaplan, Marina Barbiroli,
Franco Fuschini, Jinous Shafiei Dehkordi, Velio Tralli, Paolo Bassi and Vincenzo Petruzzelli

Abstract — **Optical wireless networks-on-chip (OWiNoC) are considered as a possible solution to overcome the communication bottleneck due to wired interconnects in modern chip multi-processor systems. The efficient implementation of optical wireless links requires considering many different aspects, including analysis and deep understanding of the effects on the propagation of the electromagnetic field induced by the discontinuities that can be found in a realistic scenario. This letter aims at showing the impact determined by some of these discontinuities on optical links designed in Silicon-on-Insulator technology, exploiting simple point-to-point interconnections as a first example. Measurements and simulations confirm that multi-path phenomena, triggered by the multi-layer structure housing the antennas and the propagation paths, can have a serious impact on the link budget, with fading effects that may compromise the performance of the link. However, in the presented experimental results, thanks to a careful choice of the chip layer structure, received powers higher than those which could have been measured for optical links fabricated in an infinite homogeneous medium are observed, thus resulting beneficial for the connection's power budget.**

Index Terms—**Optical wireless networks-on-chip, Multi-path, Finite-Difference Time-Domain.**

I. Introduction

IN order to overcome common issues, such as high latency and layout complexity, in networks-on-chip (NoC) of high density multi-core architectures, optical wireless networks on-chip (OWiNoC) have been considered as a viable solution to replace wired connections or to be integrated in wired/wireless hybrid configurations [1].

Differently from other wireless solutions proposed so far, as the millimeter-wave (mm-W) or sub-THz systems, OWiNoC allow an easy integration thanks to the micrometer/nanometer dimensions achievable for the radiating elements.

Moreover, OWiNoC can benefit from a simplified approach in modeling, and therefore controlling, the field propagation. In fact, the far-field condition between the transmitting and the receiving antennas are always verified, for typical on-chip distances, giving the chance to model the propagation for very long links without using full-wave, high-computational resources-consuming, numerical approaches [2-4].

On the other hand, OWiNoC main issues are related to the use of very small wavelengths compared to the propagation distances to cover in on-chip transmissions [5], thus requiring considerable antenna gains to compensate propagation losses.

As a consequence of this fact, the main challenges of the OWiNoC approach lie in the design of the antenna, which needs to be as much as possible easily integrable with significant gain on the horizontal plane, and in the development of a well-established knowledge of the propagation channel.

In particular, the determination of these properties is essential for the optimization of the overall wireless network (i.e. the distances between transmitters and receivers) [6], especially when complex propagation scenarios and multiple links on the same chip are implemented.

This letter focuses on the propagation channel and it highlights the importance of multi-path propagation phenomena generated by the discontinuities existing in SOI-based on-chip optical wireless links. Multi-path is responsible for extra fading and prevents the signal to be adequately received in certain regions. Measurements on simple point-to-point interconnections for different propagation distances are reported, analyzed in detail and confirmed through numerical simulations.

II. Devices fabricated and numerical analysis of the multi-path propagation

A. Fabrication description

A sketch of the fabricated device is shown in Fig. 1. It has been designed to operate in the C-band ($1530\ nm \div 1565\ nm$). and is based on the standard SOI technology.

The structure is composed of a bottom layer of Silicon of thickness $h_B = 675\ \mu m$, an overlying layer of SiO_2 of $h_S = 3\ \mu m$ height, and a further layer of Silicon of $h_{Ant} = 220\ nm$ thickness, where standard Si waveguides (with width $w_{WG} =$

J. Nanni, A. E. Kaplan, M. Barbiroli, F. Fuschini and P. Bassi are with the Department of Electrical, Electronic and Information Engineering "Guglielmo Marconi", University of Bologna, viale del Risorgimento 2, 40136 Bologna, Italy (email: jacopo.nanni3@unibo.it;aliemre.kaplan2@unibo.it; marina.barbiroli@unibo.it; franco.fuschini@unibo.it, paolo.bassi@unibo.it).

G. Bellanca, J. S. Dehkordi, V. Tralli are with the Department of Engineering, University of Ferrara, Via Giuseppe Saragat, 1, 44124 Ferrara, Italy (email: gaetano.bellanca@unife.it; shfjns@unife.it; velio.tralli@unife.it).

G.Calò, B. Alam and V. Petruzzelli are with the Department of Electrical and Information Engineering, Polytechnic of Bari, Via Edoardo Orabona, 4, 70126, Bari, Italy (email: giovanna.calo@poliba.it; badrul.alam@poliba.it; vincenzo.petruzzelli@poliba.it).

$480\ nm$) and the antennas are fabricated through Electron Beam Lithography (EBL). The antennas used for the considered links are realized by simply tapering the Si waveguides employing the same geometrical parameters presented in [7] (see Fig. 1a). Despite the not really compact dimensions, the narrow pattern on the horizontal (x-z) plane, together with the ease of manufacturing and high reliability, make this type of antenna suitable for the scope of this work, which is focused on the analysis of the effects of the propagation.

As upper layer, the presence of SiO₂ of $3\ \mu m$ thickness would represent the best solution, in order to have the dielectric antennas in the middle of an homogeneous layer bounded by air above and Silicon underneath, thus avoiding dielectric discontinuities close to the antennas. Unfortunately, the deposition of silica above the silicon waveguides and the antennas cannot guarantee a uniform surface at the top interface, preventing the possibility to control the propagation inside the chip.

Indeed, surface uniformity is important to guarantee reproducibility in fabrication and to allow, through simulations, an effective design of the optical links.
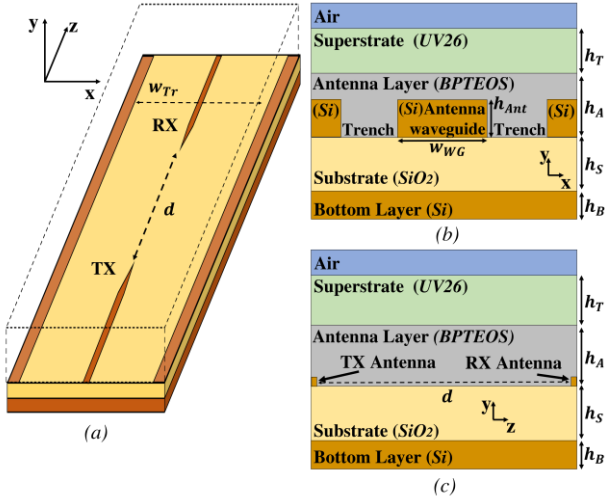

Fig. 1. 3D sketch (a) of the fabricated devices and layer structure of the sample in the *x-y* (b) and *z-y* (c) planes (see text for details).

Therefore, after etching, Silicon waveguides and antennas have been covered with a thin layer ($h_A = 300\ nm$) of borophosphorous tetraethyl orthosilicate (BPTEOS), which, contrarily to SiO₂, can be planarized through annealing process, still owing a refractive index close to the one of Silica (see Table 1).

Then, a polymer-based top layer made of UV26 of thickness $h_T = 3.78\ \mu m$ and refractive index $n_{UV26} = 1.526$ has been further deposited above the BPTEOS.

These two layers lead then to the presence of an overall quasi-homogenous medium, due to the close values of both refractive indices of these materials with the one of SiO₂.

Note that the sub-optimum solution of a single deposition of BPTEOS for a thickness of $3\ \mu m$ was not possible due to limitations in the maximum height of the coat allowed by the fabrication process. For this reason, the additional top layer has then been inserted. Among the different available polymers, the UV26 resulted to be the most suited because of the possibility

of performing a single spin-coating phase of sufficient thickness, leading to a more uniform distribution of the material on the chip. Table 1 summarizes the electromagnetic and the geometrical properties of each layer.

TABLE I
LAYER PARAMETERS

Layer	Material	Refractive index	Thickness (μm)
Bottom	Si	3.476	675
Substrate	SiO₂	1.445	3
Antenna			
- Layer	BPTEOS	1.453	0.3
- Waveguide	Si	3.437	0.22
Superstrate	UV26	1.526	3.78

To demonstrate the presence of multi-path effects, various devices have been considered on the same wafer, with a link distance d between TX and RX antennas (see Fig.1a) ranging from $20\ \mu m$ to $200\ \mu m$.

In order to ease the input and output coupling of the optical signals, standard grating couplers were realized at waveguide terminations [8], and the same grating-to-grating length (2 mm) has been maintained for all the links.

Note that, according to the EBL fabrication process, trenches must be also realized to pattern the waveguides and the antennas in the antenna layer. As shown in Fig. 1(b), these trenches create vertical discontinuities for the propagation on the horizontal x-z plane. To minimize the effects of possible lateral reflections on the received signal the trench width, w_{Tr} in Fig. 1(a), has been chosen to be $w_{Tr} = 0.6 \cdot d$, according to results obtained through numerical simulations.

B. Numerical analysis

The Finite-Difference-Time-Domain (FDTD) method [9] has been used for the numerical analysis of the optical links. For the considered link lengths ($d \leq 200\ \mu m$) and the very simple investigated scenarios, the use of a full-wave method is still possible, being time and memory requirements compatible with simulations on personal computers.

Because of its huge thickness (more than 400 times the wavelength of the optical signal), the Silicon bottom layer has been considered as infinite, inserting a Perfect Matching Layer boundary condition after an initial layer of Si of $1\ \mu m$ thickness. This also allows a strong reduction of the computation time.

The simulated link budgets (i.e. the ratio between the powers at the input and output waveguides) as a function of the link distance d and for a wavelength $\lambda = 1550\ nm$ are shown in Figure 2. Results obtained for the fabricated structure (Si-SiO₂-BPTEOS-UV26-air) are compared with the ones corresponding to a hypothetical uniform deposition above the substrate layer of $4.08\ \mu m$ SiO₂ (Si-SiO₂-SiO₂-air), therefore replacing both BPTEOS and UV26 compared to the previous case, and the ones without the UV26 layer where an air interface is present just above the antennas (Si-SiO₂-air). In this last case the SiO₂ is also considered as material for the antenna layer.

These scenarios are furthermore compared with the theoretical curve of free-space path gain (FSPG) calculated in the homogeneous medium (i.e. SiO₂ without any other material

discontinuities), obtained applying the well-known Friis equation:

$$FSPG = G_T G_R \left(\frac{\lambda}{4\pi d n_{SiO_2}}\right)^2 \qquad (1)$$

Here, the attenuation due to polarization mismatch has not been considered and the gains of the transmitting and receiving antennas, G_T and G_R respectively, have been evaluated by 3D-FDTD simulations with a single antenna surrounded by an infinite homogeneous (i.e. SiO_2) medium. In this case, the maximum obtained gain was 16.37 dB, without significant changes for the wavelengths within the C-band. The main lobe of the antenna is on the horizontal x-z plane as required for on-chip communications.
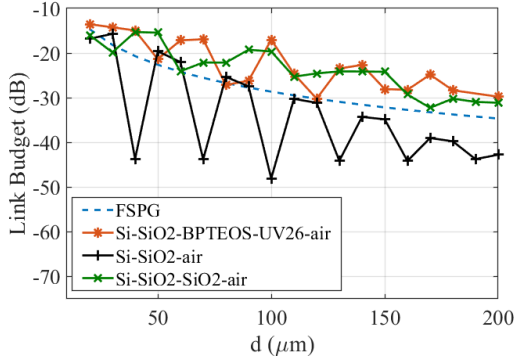

Fig. 2. Comparison of the simulated link budget for different layer configurations and for $\lambda = 1550$ *nm*.
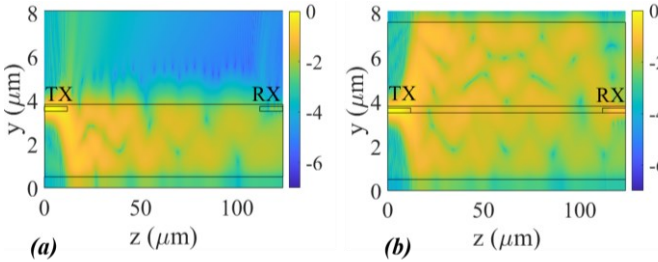

Fig. 3. Electric field pattern in the vertical y-z plane for the case of layered structure with Si-SiO2-air (a) and the one of the chip fabricated (b) where $d = 100$ μm and for $\lambda = 1550$ *nm*. The color bar represents the normalized amplitude of the electric field in logarithmic scale.

Figure 2 points out that, without any material above the antennas (i.e. keeping air as overlay), strong periodic destructive and constructive interferences on the received signal are generated. This effect is attributed to the multiple reflections which take place in the SiO_2 layer below the antennas, as it is visible from the intensity field map shown in Fig.3(a). Moreover, the corresponding curve in Fig. 2 decreases with the same trend as the FSPG, presenting important minima which can significantly reduce the received power of several dBs.

On the contrary, with the deposition of an overlayer of SiO_2 or, as for the fabricated device, BPTEOS and UV26, the link budget stays averagely above the FSPG, presenting minima which are less pronounced than the ones of the previous case, maintaining a tendency to decrease with respect to *d*.

This fact suggests that, despite the presence also in this case of multiple reflections, the average received power increases with respect to the one which would have been observed in a semi-infinite free space medium thanks to the guiding effect determined by the deposited overlay.

Results show also that the use of BPTEOS and UV26 is effective in replacing the SiO_2 above the antennas. In fact, the corresponding curves in Fig. 2 are quite similar and present both guided-like electromagnetic propagation in the antenna region.

The useful guiding effect can be further appreciated by comparing Figures 3(a) and 3(b), which show the electric field intensity in the vertical plane y-z (see also Fig. 1(c)) for both the Si-SiO2-air and the fabricated layered structure scenario, respectively. In the former case, the field is confined below the antennas because of their vicinity with the air-interface, while in the latter, guiding takes place in the layer where the antennas are located because of the more uniform refractive index distribution and geometry around them.

III. EXPERIMENTAL RESULTS AND SIMULATION COMPARISON

The experimental setup employed is shown in Fig. 4. It consists of a tunable laser source (Yenista's TLS Tunics T100) and a Yenista's CT400 passive optical component tester, which allows to evaluate the transmission coefficient $|S_{21}|^2$ of the device under test (DUT) (i.e. the ratio between the measured received power and the output power produced by the port (O) of the CT400) in the C-band. The use of an optical circulator also permits to measure the reflected power at the input port of the DUT, determining the reflection coefficient $|S_{11}|^2$. A polarization controller allows also to optimize the coupling from the fiber probe on the fundamental TE mode of the silicon waveguide.
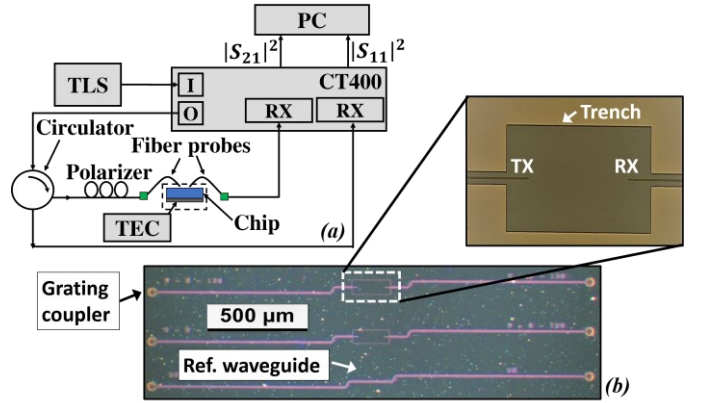

Fig. 4. (a) Experimental setup and (b) fabricated samples with an enlarged device as inset.

As previously described, fiber probes are coupled with the chip through taper gratings fabricated at the input/output sections of the waveguides, allowing an easy and repeatable coupling from the top side with an angle between the probes and the gratings of approximately 11 degrees.

In order to exclude possible undesired temperature effects on the electrical and physical parameters of the DUT, the chip is placed on a Peltier cell, isolated in an Aluminum case, controlled with an external Thermo Electric Controller (TEC). The temperature of all the measurements is fixed at 25°C.

To compensate for the losses and the wavelength response of external components, all measurements have been normalized with respect to a silicon reference waveguide of the same length fabricated on the same chip. This allows to directly obtain the

link budget of the wireless connection only, which is therefore defined as:

$$Link\ Budget_{(dB)}(d) = |S_{21}(d)|^2_{(dB)} - |S_{21,Ref}|^2_{(dB)} \quad (2)$$

where $|S_{21}(d)|^2_{(dB)}$ is the measured transmission coefficient of the DUT for different values of the distance between the antennas, while $|S_{21,Ref}|^2_{(dB)}$ represents the measurement related to the reference waveguide only.

The measured values for the link budget as a function of the distance d at $\lambda = 1550\ nm$ are shown in Figure 5. As inset, the measured reflection coefficients $|S_{11}|^2_{(dB)}$ for the reference waveguide (red curve) and for $d = 200\ \mu m$ antenna link (violet curve) are reported. These curves confirm that the antenna fabricated is well matched in the whole wavelength range of the C-band, since no appreciable difference is observed with respect to the $|S_{11}|^2$ measured on the reference waveguide. The same behavior was verified for all the link distances.

Measurements are compared in Fig. 5 with FDTD simulations and with the theoretical FSPG computed using Eq. (1). It is shown that simulations are in good agreement with the experimental results confirming, as described in Section II.B, the presence of multi-path propagation likely due to the multi-layer layout shown in Fig. 1.
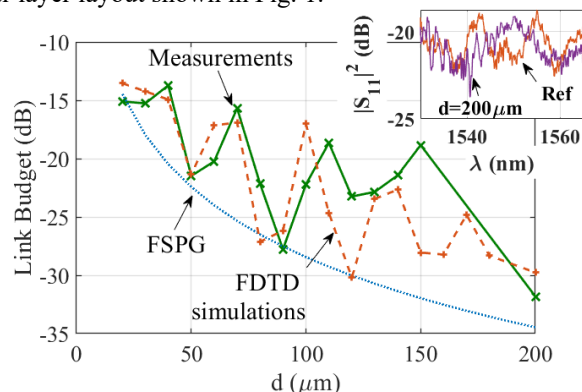

Fig. 5. Link budget as a function of the link distance d at the wavelength $\lambda = 1550\ nm$ for the measured values (green curve), the FDTD simulated values (red dashed curve), and the free space (dotted blue curve) calculated by Eq. (1). As inset, the $|S_{11}|^2$ characterization of the device at distance of 200 μm is shown compared to the one of reference waveguide.
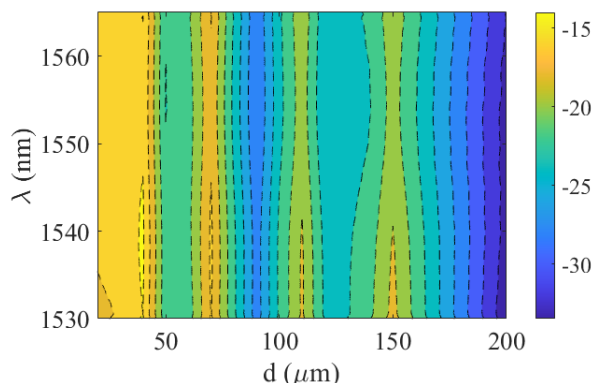

Fig. 6. Link budget measurements as a function of both link distance d and wavelength λ in the C-band range.

Guiding effect highlighted with the simulations is also confirmed. In fact, the measured link budget is higher than the one expected for propagation in homogeneous medium. However, positions where the destructive interference is important are present and located not too far from the distances foreseen by FDTD runs.

As further result, it is shown in Fig.6 that the link budget is also weakly sensitive to the wavelengths confirming that, as expected, the antenna behavior is independent on the wavelength within the C-band range [7].

IV. CONCLUSIONS

In this letter, the presence and the impact of multi-path effects in on-chip optical wireless communication has been numerically and experimentally demonstrated on simple point-to-point links for distances up to 200 μm.

Results show that the propagation on a multi-layer environment is responsible of multi-path phenomena and that an effective characterization of the wireless optical propagation channel is crucial for a proper design of the wireless link.

Positive effects on the power budget, obtained by keeping a homogeneous dielectric region hosting the antennas, have been observed, resulting on a received power higher than the one expected theoretically for the propagation in free space without interfaces. In addition, this homogeneous region around the antennas produces a reduction of the amount of fading caused by localized destructive interference along the propagation path.

REFERENCES

[1] S. Werner, J. Navaridas and M. Lujan, "A Survey on Optical Network-on-Chip Architectures, " in *ACM Comput. Surv.*, vol. 50, no. 89, 2017.

[2] F. Fuschini, M. Barbiroli, M. Zoli, G. Bellanca, G. Calò, P. Bassi and V. Petruzzelli, "Ray tracing modeling of electromagnetic propagation for on-chip wireless optical communications", *J. Low Power Electron. Appl.*, vol. 8, no. 39, 2018.

[3] S. Abadal, C. Han and J. M. Jornet, "Wave Propagation and Channel Modeling in Chip-Scale Wireless Communications: A Survey From Millimeter-Wave to Terahertz and Optics," in *IEEE Access*, vol. 8, pp. 278-293, 2020, doi: 10.1109/ACCESS.2019.2961849.

[4] M. Nafari, L. Feng and J. M. Jornet, "On-Chip Wireless Optical Channel Modeling for Massive Multi-Core Computing Architectures," *2017 IEEE Wireless Communications and Networking Conference (WCNC)*, San Francisco, CA, 2017, pp. 1-6, doi: 10.1109/WCNC.2017.7925962.

[5] G. Bellanca, G. Calò, A.E. Kaplan, P. Bassi and V. Petruzzelli, "Integrated Vivaldi plasmonic antenna for wireless on-chip optical communications," in *Optics Express*, vol. 25, no. 14, pp. 16214-16227, 2017.

[6] F. Fuschini *et al.*, "Multi-Level Analysis of On-Chip Optical Wireless Links," in *Appl. Sci.*, Vol. 10, no. 1, art no.196, 2020.

[7] C. García-Meca *et al.,*"On-chip wireless silicon photonics: from reconfigurable interconnects to lab-on-chip devices", *Light Sci Appl,* vol. 6, e17053, 2017.

[8] https://www.inphotec.it/

[9] https://www.lumerical.com